APPLIED GEOPHYSICS, Vol.13, No.1 (March 2016), P. 37-47, 9 Figures.
DOI:10.1007/s11770-016-0548-y

2.5D forward modeling and inversion of frequency-domain airborne electromagnetic data*

Li Wen-Ben[1], Zeng Zhao-Fa♦[1], Li Jing[1], Chen Xiong[1], Wang Kun[1], and Xia Zhao[1]

Abstract: Frequency-domain airborne electromagnetics is a proven geophysical exploration method. Presently, the interpretation is mainly based on resistivity–depth imaging and one-dimensional layered inversion; nevertheless, it is difficult to obtain satisfactory results for two- or three-dimensional complex earth structures using 1D methods. 3D forward modeling and inversion can be used but are hampered by computational limitations because of the large number of data. Thus, we developed a 2.5D frequency-domain airborne electromagnetic forward modeling and inversion algorithm. To eliminate the source singularities in the numerical simulations, we split the fields into primary and secondary fields. The primary fields are calculated using homogeneous or layered models with analytical solutions, and the secondary (scattered) fields are solved by the finite-element method. The linear system of equations is solved by using the large-scale sparse matrix parallel direct solver, which greatly improves the computational efficiency. The inversion algorithm was based on damping least-squares and singular value decomposition and combined the pseudo forward modeling and reciprocity principle to compute the Jacobian matrix. Synthetic and field data were used to test the effectiveness of the proposed method.
Keywords: Frequency-domain airborne electromagnetic, finite element method, 2.5D geo-electric model, damped least-squares method

Introduction

Airborne electromagnetic methods are based on the electrical and magnetic properties of rocks and take advantage of the electromagnetic induction principle. Typically, fixed-wing aircrafts or helicopters are used as instrument carriers. Airborne electromagnetic methods are efficient, economical, and easily adaptable, especially in large-scale mineral exploration (Li, 2008).

Various methods are used in electromagnetic (EM) modeling, e.g., integral-volume method, finite-difference method, and finite-element method. The latter can easily model irregular and complex geometries. The literature is full of examples of airborne electromagnetic simulations. Liu and Benker (1992) evaluated the effect of topography on helicopter EM surveys using the boundary element method. Newman and Alumbaugh (1995) simulated the 3D helicopter EM response using the finite-difference method. Tan (2010) developed a

Manuscript received by the Editor March 25, 2015; revised manuscript received March 2, 2016.
*This work was supported by the Doctoral Fund Project of the Ministry of Education (No. 20130061110060 class tutors), the National Natural Science Foundation of China (No. 41504083), and National Basic Research Program of China (973 Program) (No. 2013CB429805).
1. College of Geo-exploration Science and Technology, Jilin University, Changchun 130026, China.
♦Corresponding author: Zeng Zhao-Fa (Email: zengzf@jlu.edu.cn)

2.5D frequency-domain airborne EM numerical software based on the finite-element method. Li (2011) presented a 2D parallel algorithm for frequency-domain airborne EM using the finite-element method, which improved the computation efficiency. Zhou (2011) and Wang (2013) evaluated the 2D responses of airborne transient electromagnetic using the finite-element method. Yin (2012) simulated the airborne transient electromagnetic responses using a 2D model that included topography. Yin et al. (2015b) used a 2.5D unstructured finite-element model for transient electromagnetics and considered the strong effect of topography on the electromagnetic response.

Airborne electromagnetic method interpretation is mainly based on 1D inversion, because 2D or 3D inversion simulations are difficult to build and to make them account for the complexity of airborne EM surveys. Therefore, the conductivity-depth transform (Huang and Fraser, 1996, 2002; Sengipel, 1988) was used to obtain the subsurface conductivity distribution in airborne electromagnetic data. Owing to the low resolution of the conductivity-depth transform, many 1D methods, such as the layered earth inversion (Chen and Raiche, 1998; Farquharson et al., 2003; Huang and Fraser, 2003; Zhou et al., 2010; Yin and Hodges, 2007), the laterally constrained layered earth inversion (Auken et al., 2005; Tartaras and Beamish, 2005; Vallée and Smith, 2009; Viezzoli et al., 2009; Cai et al., 2014), and the holistic inversion (Brodie and Sambridge, 2006, 2009) are used. Despite the widespread use of 1D methods for the interpretation of AEM surveys, they often fail to recover simple 2D or 3D targets, particularly where complex 2D or 3D geological conditions are present (Ellis, 1998; Raiche et al., 2001; Wilson et al., 2006).

Several studies have tried to solve the above mentioned problem by using 2D and 3D inversion of frequency-domain airborne electromagnetics (FAEM) surveys. Wilson et al. (2006) presented a 2.5D inversion algorithm for the transient electromagnetic method using synthetic and field data to demonstrate the effectiveness of their algorithm. Cox et al. (2010) used a 3D FAEM survey of field data and the conjugate gradient method to minimize an objective functional based on an integral equation. Liu and Yin (2013) used the nonlinear conjugate gradient method and synthetic data to show the applicability of their method. Yi and Sasaki (2015) improved the inversion quality by the joint inversion of FAEM and direct current resistivity data. However, the primary problem with 3D inversion is the necessity to solve as many large linear equations as the FAEM stations because of computer memory constraints (Yin et al., 2015a). 2.5D inversion algorithms can well recover the 2D geological complexities with better computational efficiency than 3D inversion methods.

In this study, we first discuss a 2.5D forward modeling algorithm based on the isoparametric finite-element and Galerkin's method. Based on the forward modeling algorithm, we develop a damped least-squares inversion method using singular value decomposition (SVD). Finally, we test the proposed algorithm using synthetic and field data.

2.5D forward modeling of frequency-domain airborne electromagnetics

The 2.5D problem derives from the fact that the source is 3D and the model is 2D. As shown in Figure 1, the anomalous body striking in the y-direction is extended infinitely, the conductivity σ, permittivity ε, and magnetic permittivity μ are constant along strike and only vary in the xz plane. The transmitter and receiver are approximately 30 m above the earth surface. Assuming harmonic temporal dependency with $e^{i\omega t}$, the electric and magnetic fields satisfy Maxwell's equations (Ward and Hohmann, 1988)

$$\nabla \times \mathbf{E} = -\hat{z}\mathbf{H} - \hat{z}\mathbf{M}_s, \tag{1a}$$

$$\nabla \times \mathbf{H} = \hat{y}\mathbf{E} + \mathbf{J}_s, \tag{1b}$$

where $\mathbf{M}_s$ and $\mathbf{J}_s$ are the magnetic and electric sources, respectively, $\hat{z} = i\omega\mu$ is the impedance, and $\hat{y} = \sigma + i\omega\varepsilon$ is the admittivity.

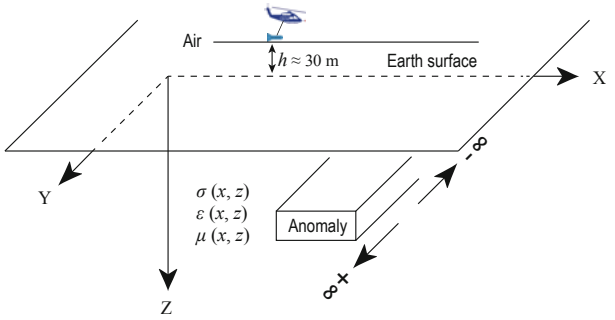

Fig.1 2.5D geoelectrical model along the y-direction.

The space between the transmitter and receiver in frequency-domain airborne electromagnetics are small; moreover, we cannot obtain exact results even when using a refined grid because the electric and magnetic

fields quickly change near the source. To eliminate the source singularities in the numerical simulation, we split the fields into primary and secondary (Newman and Alumbaugh, 1995)

$$\mathbf{E} = \mathbf{E}^p + \mathbf{E}^s, \tag{2a}$$

$$\mathbf{H} = \mathbf{H}^p + \mathbf{H}^s, \tag{2b}$$

where superscripts p and s denote the primary and secondary field, respectively. The magnetic permeability μ is considered constant and equal to the magnetic permeability in vacuum and, ignoring the displacement currents, the secondary Maxwell's equations can be written as

$$\nabla \times \mathbf{E}_s = -i\omega\mu_0 \mathbf{H}_s, \tag{3a}$$

$$\nabla \times \mathbf{H}_s = \sigma \mathbf{E}_s + \mathbf{J}_s, \tag{3b}$$

where $\mathbf{J}_s = (\sigma - \sigma_p)\mathbf{E}_p$ and σ_p is the background conductivity. Applying the Fourier transform to equations (3a) and (3b) with respect to y yields

$$\hat{F}(x,k_y,z,\omega) = \int_{-\infty}^{+\infty} F(x,y,z,\omega)e^{-ik_y y}dy, \ \frac{\partial \hat{F}}{\partial y} = -ik_y \hat{F}, \tag{4}$$

where $\hat{F}$ denotes $\hat{E}_x^s$, $\hat{E}_y^s$, $\hat{E}_z^s$, $\hat{H}_x^s$, $\hat{H}_y^s$, and $\hat{H}_z^s$ in the wave domain. We obtain the two coupled governing differential equations for $\hat{E}_y^s$ and $\hat{H}_y^s$

$$-\frac{\partial}{\partial x}(p\frac{\partial \hat{H}_y^s}{\partial x}) - \frac{\partial}{\partial z}(p\frac{\partial \hat{H}_y^s}{\partial z}) - \frac{\partial}{\partial x}(-q\frac{\partial \hat{E}_y^s}{\partial z}) - \frac{\partial}{\partial z}(q\frac{\partial \hat{E}_y^s}{\partial x}) - i\omega\mu_0 \hat{H}_y^s = \hat{S}_1, \tag{5a}$$

$$-\frac{\partial}{\partial x}(q\frac{\partial \hat{H}_y^s}{\partial z}) - \frac{\partial}{\partial z}(-q\frac{\partial \hat{H}_y^s}{\partial x}) - \frac{\partial}{\partial x}(r\frac{\partial \hat{E}_y^s}{\partial x}) - \frac{\partial}{\partial z}(r\frac{\partial \hat{E}_y^s}{\partial z}) - \sigma \hat{E}_y^s = \hat{S}_2, \tag{5b}$$

where

$$p = \frac{i\omega\mu_0}{k^2 - k_y^2}, \ q = \frac{ik_y}{k^2 - k_y^2}, \ r = \frac{\sigma}{k^2 - k_y^2},$$

$$k^2 = -i\omega\mu_0\sigma, \ \hat{S}_1 = \frac{\partial}{\partial z}(p\sigma_a \hat{E}_x^p) - \frac{\partial}{\partial x}(p\sigma_a \hat{E}_z^p),$$

and

$$\hat{S}_2 = \sigma_a \hat{E}_y^p + \frac{\partial}{\partial x}(q\sigma_a \hat{E}_x^p) + \frac{\partial}{\partial z}(q\sigma_a \hat{E}_z^p).$$

The rest of the electric and magnetic fields can be calculated from the space derivatives of $\hat{E}_y^s$ and $\hat{H}_y^s$

$$\hat{E}_x^s = q\frac{\partial \hat{E}_y^s}{\partial x} + p\frac{\partial \hat{H}_y^s}{\partial z} + p\sigma_a \hat{E}_x^p, \tag{6}$$

$$\hat{E}_z^s = -p\frac{\partial \hat{H}_y^s}{\partial x} + q\frac{\partial \hat{E}_y^s}{\partial z} + p\sigma_a \hat{E}_z^p, \tag{7}$$

$$\hat{H}_x^s = q\frac{\partial \hat{H}_y^s}{\partial x} - r\frac{\partial \hat{E}_y^s}{\partial z} - q\sigma_a \hat{E}_z^p, \tag{8}$$

$$\hat{H}_z^s = r\frac{\partial \hat{E}_y^s}{\partial x} + q\frac{\partial \hat{H}_y^s}{\partial z} + q\sigma_a \hat{E}_x^p, \tag{9}$$

where $\sigma_a = \sigma - \sigma_p$.

Maxwell's equations are solved by using the finite-element and Galerkin's method (Zienkiewicz, 1977). We apply Garlerkin's method to equations (5a) and (5b) and assemble the elemental matrices in a global matrix; thus, we obtain the global set of equations, (for details, see Appendix A)

$$\mathbf{K}\hat{\mathbf{F}} = \mathbf{B}, \tag{10}$$

where $\mathbf{K}$ is a sparse symmetric system matrix, $\hat{\mathbf{F}}$ is the representation of the unknown EM fields, and $\mathbf{B}$ represents the source term.

The secondary fields decay to zero at the boundaries far from the anomaly. To ensure the uniqueness of the solution, we consider the simple Dirichlet's boundary condition and zero the fields at the boundary. To decrease the boundary effects in the simulations, the boundaries are set far from the area of interest by increasing the node spacings with a ratio of 1:2. The system of linear equations (10) can be iteratively (e.g., QMR, Newman and Alumbaugh, 1995) or directly solved (e.g., MUMPS, Streich, 2009). Iterative solvers require less memory than direct solvers. They also require less computational time when only one right-hand side is computed and the matrix factorization of direct solvers is expensive. However, the iterative solvers of typical multisource frequency-domain airborne electromagnetics are expensive. For several right-hand side equations, directive solvers are inexpensive because matrix factorization can be reused. Therefore, the system of linear equations was solved by the large-scale spare matrix parallel direct solver (PARDISO).

Once $\hat{E}_y^s$ and $\hat{H}_y^s$ are computed, other field components can be obtained using equations (6) and (9). These complementary components are calculated from the space derivatives of $\hat{E}_y^s$ and $\hat{H}_y^s$, which are evaluated

from the space derivatives of the interpolation function $\partial N_i^e/\partial x$ and $\partial N_i^e/\partial z$ for each element, where N_i^e is the elementary shape function (Zienkiewicz, 1977). The EM fields in the k_y-domain are transformed to the space domain by the inverse Fourier transform (Leppin 1992; Unsworth et al., 1993)

$$F(x, y = y_0, z, \omega) = \frac{1}{\pi}\int_0^{+\infty} \hat{F}(x, k_y, z, \omega) e^{ik_y} dk_y. \quad (11)$$

The inverse Fourier transform is evaluated by the sine or cosine transform with a filtering algorithm.

Primary field

In this study, the primary fields are calculated in uniform whole space by using analytical expression. Due to the high accuracy and computational efficiency, compared with layered model.

In the vertical coaxial configuration, the source is a horizontal magnetic dipole in the x-direction and the primary field is evaluated as follows (Nabighian, 1991):

$$E_x^p = 0, \quad (12a)$$

$$E_y^p = \frac{i\omega\mu m}{4\pi r^2} \cdot (ikr + 1) \cdot e^{-ikr} \cdot \frac{z}{r}, \quad (12b)$$

$$E_z^p = -\frac{i\omega\mu m}{4\pi r^2} \cdot (ikr + 1) \cdot e^{-ikr} \cdot \frac{y}{r}. \quad (12c)$$

In the horizontal coplanar configuration, the source is a vertical magnetic dipole and the primary field is computed as follows (Nabighian, 1991):

$$E_x^p = \frac{i\omega\mu m}{4\pi r^2} \cdot (ikr + 1) \cdot e^{-ikr} \cdot \frac{y}{r}, \quad (13a)$$

$$E_y^p = -\frac{i\omega\mu m}{4\pi r^2} \cdot (ikr + 1) \cdot e^{-ikr} \cdot \frac{x}{r}, \quad (13b)$$

$$E_z^p = 0. \quad (13c)$$

The primary fields in the space domain are transformed into the wave domain by the Fourier transform. The latter can be evaluated by the sine or cosine transform because of the odd or even symmetry of the primary fields.

Verification of the 2.5D forward modeling

To verify the precision of the 2.5D forward modeling algorithm, we consider the model of Newman and Alumbaugh (1995) in Figure 2a. The results are shown in Figures 2b and 2c horizontal coplanar (HCP) and vertical coaxial (VCX) systems, respectively, and agree well with Newman's results. The maximum relative error is only 4%, which suggests that the 2.5D forward modeling can be used in the inversion.

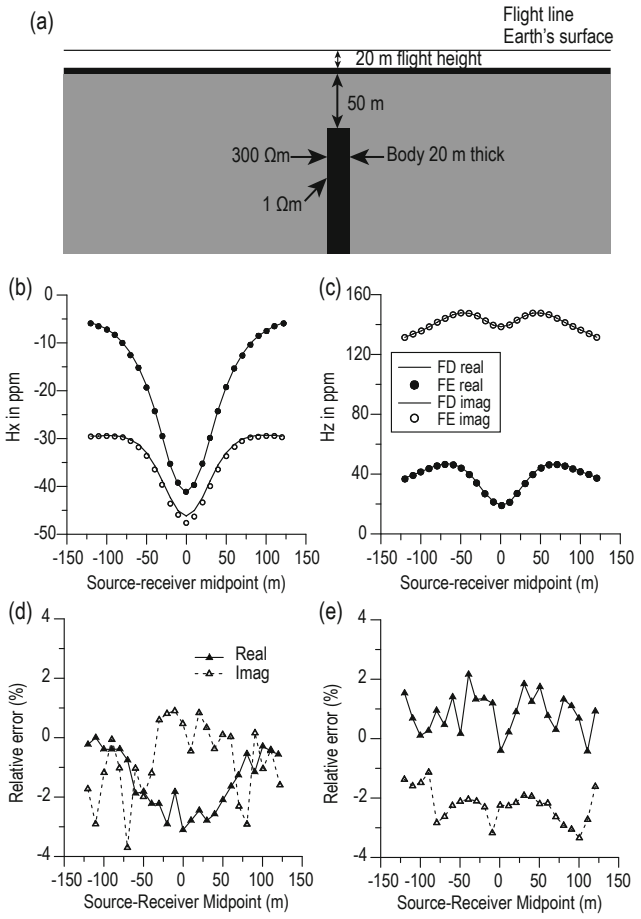

Fig.2 Comparison of the 2.5D model results using the data of Newman (1995). (a) 2D model. The VCX and HCP results are shown in (b) and (c), respectively. The relative error for VCX and HCP is shown in (d) and (e), respectively.

Damped least-squares 2.5D inversion

The damped least-squares inversion algorithm

The damped least-squares method is the classic Marquardt's method and is based on least-squares criteria. The method seeks the optimal solution by minimizing the residuals of an objective function. In the frequency-domain airborne electromagnetic inversion, the objective function is

$$\Phi(\mathbf{p}) = \frac{1}{N}\sum_{i=1}^{N}\left[(F_i(\mathbf{p}) - d_i^{obs}) / \sigma_i\right]^2, \quad (14)$$

where $\mathbf{d} = [d_1, d_2, \cdots, d_N]^T$ is the measured data vector,

$\mathbf{p} = [p_1, p_2, \cdots, p_M]^T$ is the unknown model parameters vector, T is the transpose, N is the number of measured data, and M is the number of model parameters. The functional relation between the model parameters and EM responses is

$$d_i^{obs} = F_i(\mathbf{p}), i = 1, 2, \cdots, N. \quad (15)$$

In the frequency-domain airborne electromagnetic problem, the function $F_i(\mathbf{P})$ is strongly nonlinear. To locally linearize the problem, we expand $F_i(\mathbf{P})$ using Taylor series around the initial model parameter vector $\mathbf{p}^0$ for the first iteration and neglect the higher order terms. Thus, we obtain

$$\Delta\mathbf{d} = \mathbf{J}\Delta\mathbf{p}, \quad (16)$$

where $\Delta\mathbf{d}$ is the vector of differences between the measured data and the response of the initial model, and $\Delta\mathbf{p}$ is the vector to be solved, comprising the difference between the updated and initial model parameters $\mathbf{p}$ and $\mathbf{p}^0$. $\mathbf{J}$ is an $N \times M$ Jacobian or sensitivity matrix with elements

$$a_{ij} = \frac{\partial F_i(\mathbf{p})}{\partial p_j}, i = 1, 2, \cdots, N, j = 1, 2, \cdots, M. \quad (17)$$

From this, we obtain the model update step

$$\Delta\mathbf{p} = (\mathbf{J}^T\mathbf{J})^{-1} \cdot \mathbf{J}^T\Delta\mathbf{d}. \quad (18)$$

Because of the singularities in the coefficient matrix, the inversion is unstable. To correct this, we add the damped factor λ^2 into the coefficient matrix

$$(\mathbf{J}^T\mathbf{J} + \lambda^2\mathbf{I})\Delta\mathbf{p} = \mathbf{J}^T\Delta\mathbf{d}, \quad (19)$$

where $\mathbf{I}$ is the identity matrix. Using SVD, we obtain

$$\mathbf{J} = \mathbf{U}\mathbf{\Lambda}\mathbf{V}^T, \quad (20)$$

where $\mathbf{U}$ and $\mathbf{V}$ is the data and parameter eigenvector matrix, respectively, and Λ is the singular values matrix. Substituting equation (20) into (19), we obtain

$$\Delta\mathbf{p} = \mathbf{V}(\mathbf{\Lambda}^2 + \lambda^2\mathbf{I})^{-1}\mathbf{\Lambda}\mathbf{U}^T\Delta\mathbf{d}, \quad (21)$$

Then, the updated model parameter vector at the kth iteration is

$$\mathbf{p}^k = \mathbf{p}^{k-1} + \Delta\mathbf{p}. \quad (22)$$

In the case of nonlinear problems, several iterations are required before an acceptable solution is obtained by minimizing the misfit between data and model responses.

Jacobian matrix

The calculation of the Jacobian matrix is critical in the inversion algorithm, and the computational efficiency strongly affects the inversion efficiency. There are simple and effective methods for this purpose (McGillivary et al, 1994; Lugão and Wannamaker,, 1996). In this study, we use the reciprocity principle to calculate the Jacobian matrix and minimize the computation time. We differentiate both sides of equation (10) with respect to the conductivity of a particular block σ_i and we obtain

$$\mathbf{K}\frac{\partial\hat{\mathbf{F}}}{\partial\sigma_i} = -\frac{\partial\mathbf{K}}{\partial\sigma_i}\hat{\mathbf{F}}. \quad (23)$$

This equation has the same coefficient matrix with the 2.5D forward model; moreover, the right-hand side can be seen as the source term and the derivatives of the electric field with respect to σ_i can be obtained by solving equation (23), which resembles the forward modeling and is called pseudo forward modeling. We repeat the pseudo forward modeling N times to obtain the derivatives of the electric field for N blocks of conductivity, which is time-consuming. However, in the inversion algorithm, we only need the derivatives of the electric field with respect to the conductivity at the receiving point. Using the reciprocity (Lugão and Wannamaker, 1996), the derivative of the electric field at the receiving point is the weighted sum of the electric fields within the block owing to the unit dipole source at the receiver point (for details, see Appendix B).

Inversion scheme

The 2.5D frequency-domain airborne electromagnetic inversion algorithm comprises the following steps (shown in Figure 3).

1. Set the iteration number $i = 0$, the threshold for the residual, and the maximum iteration number and input the initial model parameters and measured data.
2. Perform the 2.5D forward calculations, solve the system of linear equations $\mathbf{K}\hat{\mathbf{F}} = \mathbf{B}$ and obtain the secondary magnetic fields H_x and H_z.
3. Calculate the residual. If the residual is satisfactory or the iteration number is greater than the maximum iteration number, exit the program; otherwise, continue.
4. Search for the best damping factor.
5. Use the pseudo forward modeling model to calculate the Jacobian matrix and obtain the update step.
6. Update the model parameter $\mathbf{p}^{k+1} = \mathbf{p}^k + \Delta\mathbf{p}$.
7. Set $i = i + 1$ and return to step 2.

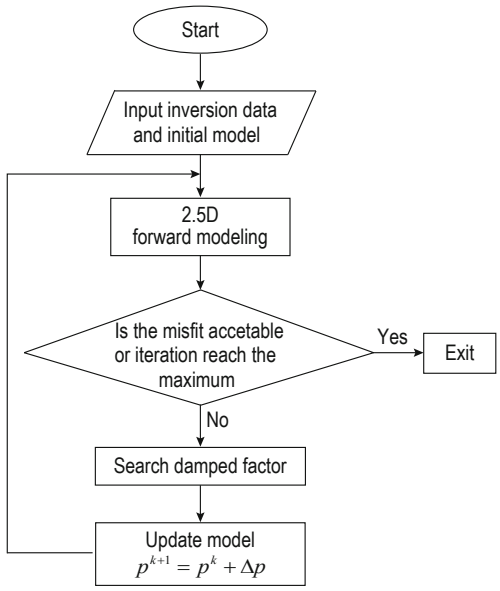

Fig.3 2.5D frequency-domain airborne electromagnetic inversion flowchart.

Inversion of synthetic data

To test the application and correct the damped least-squares inversion algorithm, we use two typical geoelectrical models.

Model No. 1

Model No. 1 is shown in Figure 4. The model size is 1200 m × 250 m and contains two 20 ohm-m low-resistivity bodies buried in 200 ohm-m half-space. The anomaly size is 150 m × 80 m and the distance from the top surface to the earth surface is 40 m. The transmitter and receiver loops are assumed to be 6.5 m apart and 30 m above the earth's surface. The magnetic field response was computed using a 42 × 13 cell grid for 50 locations at intervals of 20 m. The frequencies for the HCP and VCX were 930 Hz, 4650 Hz, and 23250 Hz and 870 Hz, 4350 Hz, and 21750 Hz, respectively.

The starting model was a homogeneous 200 ohm-m half-space. Before the inversion, the 50 locations of the HCP and VCX configurations for six frequencies were contaminated with 1% Gaussian noise. For the 2.5D inversion algorithm, we used a desktop computer with a 3.5 GHz Intel (R) Core (TM) i3-4150 processor. The data misfit was reduced from 100% to 7.34% after 15 iterations and 5.2 h. The inversion results are shown in Figure 5, which suggests that the recovered resistivity is reasonably well represented by the model.

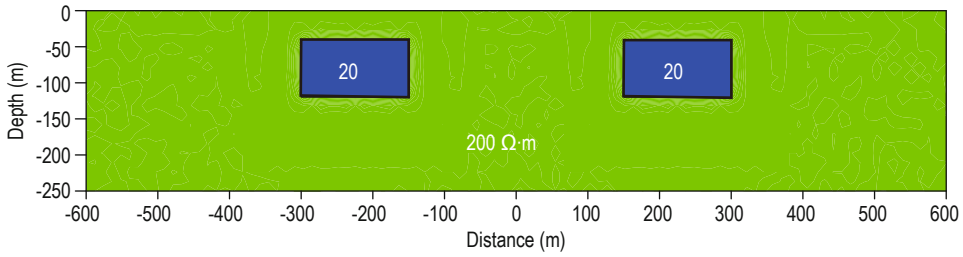

Fig.4 2D model used to generate the synthetic data for the frequency-domain airborne EM survey. The model comprises two buried blocks of 20 ohm-m in 200 ohm-m background half-space.

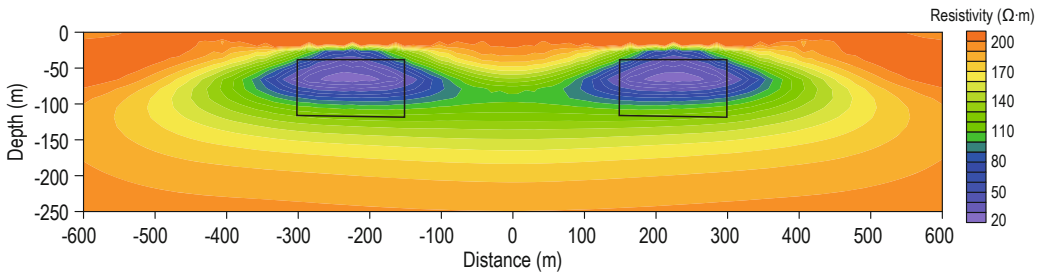

Fig.5 Resistivity model obtained from inverting the frequency-domain airborne EM data for the model in Figure 4.

Model No. 2

Model No. 2 comprises two rectangular, 20 ohm-m and 2000 ohm-m, bodies in 200 ohm-m background half-space, as shown in Figure 5. The inversion results were generated using the same parameter as in model No. 1. The data misfit was reduced from 100% to 9.34%

after 11 iterations and approximately 3.8 h.

The inversion results are shown in Figure 7. The low resistivity is well recovered as well as the high resistivity but the latter is only 300 ohm-m, which is far from the true value of 2000 ohm-m. The airborne EM system records the secondary magnetic fields generated by the anomaly and it is not sensitive to the high-resistivity anomaly. Oldenburg et al. (2012) considered this result unsurprising because it is difficult to recover a high-resistivity body by using an induced source and magnetic field data.

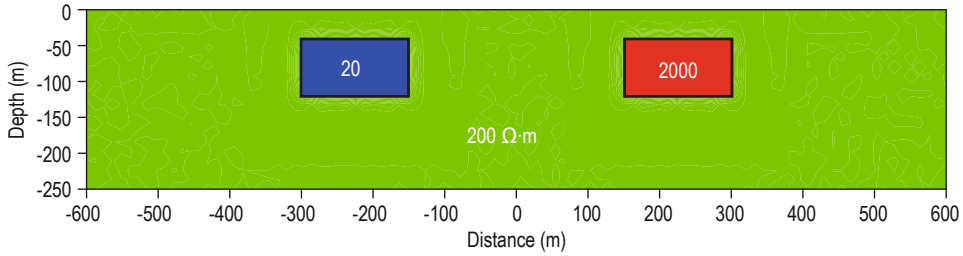

Fig.6 2D model used to generate the synthetic data for frequency-domain airborne EM survey. The model comprises two, 20 ohm-m and 2000 ohm-m, buried blocks in 200 ohm-m background half-space.

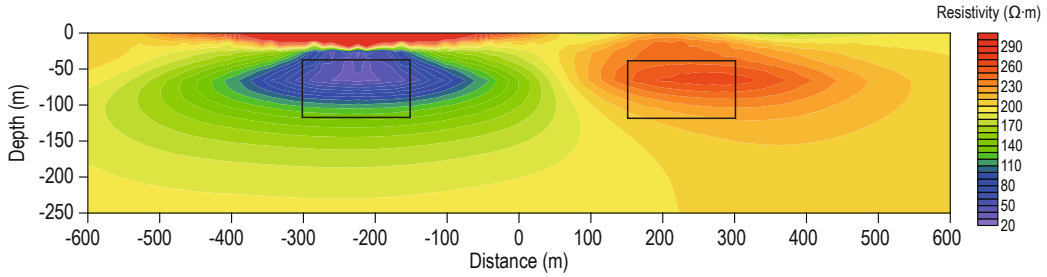

Fig.7 Resistivity model obtained from inverting the frequency-domain airborne EM data for the model in Figure 6.

Field example

We used field data to test the proposed inversion algorithm. The field data were from the Guangdong Longmen area and were collected with the IMPULSE airborne electromagnetic system and targeted zinc, lead, and copper deposits. The rocks are mainly Neoproterozoic, Cambrian, Devonian, Carboniferous, Permian, Mesozoic Triassic, Jurassic, Cretaceous and Cenozoic in age. The intrusive rocks are mainly from the Yanshanian period, wherein the third and the fourth stages are granite and the fifth stage is granite porphyry. The area is rich in mineral resources. The lead and zinc deposits are associated with contact metasomatic skarn, hydrothermally altered hornfels, or stratiform hydrothermal alteration. The resistivity of the Mesozoic granite and sedimentary rocks is hundreds to thousands ohm-m and the resistivity of the dense veins is tens to hundreds ohm-m (Wang et al., 2007).

The field data inversion profile is 700 m long covering 281 locations with an average interval of 2.3 m. The inversion data use the HCP configuration with three frequencies (930 Hz, 4650 Hz, and 23250 Hz). The inversion region was divided into 35 × 12 blocks of unknown parameters, excluding the air layer. The inversion results are shown in Figure 8. The FAEM inversion results well agree with the CSAMT data. Between 300 m and 500 m of the recovered

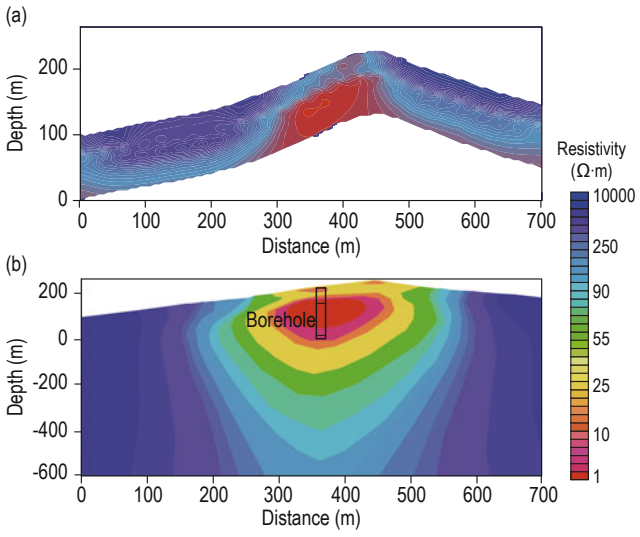

Fig.8 Comparison of the (a) AEM and (b) CSAMT inversion results (Hu et al., 2013).

resistivity profile, the low-resistivity anomaly follows the mineralization in the Longmen area (Wang et al., 2007). A borehole was drilled at the location of 370 m of this profile to investigate the central conductive body. The borehole depth is about 250 m, and continuous pyrite was discovered at the depth 52–235 m, chemical component analysis indicated Fe content of 7%–16%, (Hu et al., 2013).

Conclusions

We presented a 2.5D frequency-domain airborne electromagnetic forward modeling and inversion algorithm. To eliminate the point-source singularities in the numerical simulation, the fields are split into primary and secondary fields. The primary fields are computed analytically using layered or homogeneous models and the secondary fields are solved by using the isoparametric finite-element and Galerkin's method. The system of linear equations was solved by using the parallel direct solver PARDISO, which solved the multi-right-hand side problem efficiently. We developed a damped least square inversion algorithm based on SVD and computed the Jacobian matrix using a pseudoforward model and the reciprocity principle. We used synthetic and field data to test the effectiveness of the proposed algorithm.

References

Auken, E., Chistiansen, A. V., Jacobsen, B. H., et al., 2005, Piece-wise 1D laterally constrained inversion of resistivity data: Geophysical Prospecting, **53**, 497−506.

Brodie, R., and Sambridge, M., 2006, A holistic approach to inversion of frequency-domain airborne EM data: Geophysics, **71**(6), G301−G312.

Brodie, R., and Sambridge, M., 2009, Holistic inversion of frequency-domain airborne electromagnetic data with minimal prior information: Exploration Geophysics, **40**, 8−16.

Cai, J., Qi, Y. F., Yin, C. C., et al., 2014, Weighted Laterally-constrained inversion of frequency-domain airborne EM data: Chinese Journal of Geophysics, **57**(1), 953−960.

Chen, J., and Raiche, A., 1998, Inverting AEM data using a damped eigenparameter method: Exploration Geophysics, **29**, 128−132.

Cox, L. H., Wilson, G. A., and Zhdanov, M. S., 2010, 3D inversion of airborne electromagnetic data using a moving footprint: Exploration Geophysics, **41**, 250−259.

Ellis, R. G., 1988, Inversion of airborne electromagnetic data: Exploration Geophysics, **29**, 121−127.

Farquharson, C. G., Oldenburg, D. W., and Routh, P. S., 2003, Simultaneous 1-D inversion susceptibility and electrical conductivity: Geophysics, **68**(6), 1857−1869.

Huang, H. P., and Fraser, D. C., 1996, The differential parameter method for multifrequency airborne resistivity mapping: Geophysics, **61**(1), 100−109.

Huang, H. P., and Fraser, D. C., 2002, Dielectric permittivity and resistivity mapping using high frequency helicopter-borne EM data: Geophysics, **67**(3), 727−738.

Huang, H. P., and Fraser, D. C., 2003, Inversion of helicopter electromagnetic data to a magnetic conductive layered earth: Geophysics, **68**(4), 1211−1223.

Hu, X. Y., Peng R. H., Wu, G. J., et al., 2013, Mineral Exploration using CSAMT data: Application to Longmen region metallogenic belt, Guangdong Province, China: Geophysics, **78**(3), B111−B119.

Leppin, M., 1992, Electromagnetic modeling of 3-D source over 2D inhomogeneities in the time domain: Geophysics, **57**(8), 994−1003.

Li, X. K., 2011, A MPI Based Parallel Calculation Investigation on Two Dimensional Finite Element Modelling of AEM: PhD Thesis, China University of Geosciences, Beijing.

Li, W. J., 2008, Data Processing of Frequency Domain Airborne Electromagnetic Survey: PhD Thesis, China University of Geosciences, Beijing.

Liu, G. M., and Becker, A., 1992, Evaluation of terrain effects in AEM survey suing the boundary element method: Geophysics, **57**(2), 272−278.

Liu, Y. H., and Yin, C. C., 2013, 3D inversion for frequency-domain HEM data: Chinese Journal of Geophysics, **56**(12), 4278−4287.

Lugão, P. P., and Wannamaker, P. E., 1996, Calculating the two-dimensional magnetotelluric Jacobian in finite elements using reciprocity: Geophys. J. Int., **127**, 806−810.

McGillivaray, P. R., Oldenburg, D. W., Ellis R. G., et al., 1994, Calculation of sensitivity for the frequency-domain electromagnetic problem: Geophys. J. Int., **116**, 1−4.

Nabighian, M. N., 1991, Electromagnetic theory for geophysical applications Electromagnetic Methods in Applied Geophysical: Vol.1, Theory, Geological Publishing House, 164−165.

Newman, G. A., and Alumbaugh, D. L., 1995, Frequency domain modeling of airborne electromagnetic responses using staggered finite differences: Geophysical Prospecting, **43**, 1021−1042.

Oldenburg, D. W., Haber, E., and Shekhtman R., 2013,

Three Dimensional inversion of multisource time domain electromagnetic data: Geophysics, **78**(1), 47−57.

Raiche, A., Annetts, D., and Sugeng, F., 2001, EM target response in complex hosts: Presented at ASEG 15th Geophysical Conference and Exhibition, Brisbane.

Sengpiel, K. P., 1988, Approximate inversion of airborne EM data from a multilayered ground: Geophysical Prospecting, **36**(4), 446−459.

Streich, R., 2009, 3D finite-difference frequency-domain modeling of controlled-source electromagnetic data: Direct solution and optimization for high accuracy. Geophysics **74**, F95–F105.

Tan, L., 2010, 2.5D numerical simulation software developing of Frequency domain AEM: MSc Thesis, China University of Geosciences, Beijing.

Tartaras, E., and Beamish, D., 2005, Laterally-constrained inversion of fixed-wing frequency-domain AEM data: Presented at 12th European Meeting of Environmental and Near Surface Geophysics, Helsinki.

Unsworth, M. J., Travis, B. J., and Chave, A. D., 1993, Electromagnetic induction by a finite electric dipole source over a 2-D earth: Geophysics, **58**, 198−214.

Vallée, M. A., and Smith, R. S., 2009, Inversion of airborne time-domain electromagnetic data to a 1D structure using lateral constraints: Near Surface Geophysics, **7**, 63−71.

Viezzoli, A., Auken, E., and Munday T., 2009, Spatially constrained inversion for quasi 3D modeling of airborne electromagnetic data-an application for environmental in the Lower Murray Region of South Australia: Exploration Geophysics, **40**, 173−183.

Wang, W. P., Fang, Y. Y., and Zheng G. R, 2007, The exploration efficiency of the helicopter electromagnetic system in Longmen, Guangdong province: Geophysical & Geochemical exploration, **31**(6), 546−550.

Wang, Y. H., 2013, The Research on HTEM 2.5D Forward Modeling and Curve Analysis: MSc Thesis, Chendu University of Technology.

Ward, S. H., and Hohmann, G. W., 1988, Electromagnetic theory for geophysical applications Electromagnetic Methods in Applied Geophysical: Vol.1, Theory, in Nabighian, M. N., Ed., Society of exploration geophysics, 131−311.

Wilson, G. A., Raiche, A. P., and Sugeng F., 2006, 2.5D inversion of airborne electromagnetic data: Exploration Geophysics, **37**, 363−371.

Yin, C. C., and Hodgres, G., 2007, Simulated annealing for airborne EM inversion; Geophysics, **72**(4), F189−F196.

Yin, C. C., Ren, X. Y., Liu, Y. H., et al., 2015a, Review on airborne electromagnetic inversion theory and applications, Geophysics, **80**(4), W17–W31.

Yin, C. C., Zhang, B., Liu, Y. H., et al., 2015b, 2.5-D forward modeling of the time-domain airborne EM system in areas with topographic relief: Chinese J. Geophys. (in Chinese), **58**(4), 1411–1424.

Yin, H. J., 2012, 2.5D forward of time-domain of airborne electromagnetic: MSc Thesis, China University of Geosciences, Beijing.

Yi, M. J., and Sasaki, Y., 2015, 2-D and 3-D joint inversion of loop-loop electromagnetic and electrical data for resistivity and magnetic susceptibility: Geophys. J. Int., **203**, 1085–1095.

Zhou, D. Q., Tan, L., Tan, H. D., et al., 2010, Inversion of frequency domain helicopter-borne electromagnetic data with Marquardt's method: Chinese Journal of Geophysics, **56**(2), 421−427.

Zhou, J. J., 2011, Research on Airborne Transient Electromagnetic 2.5D Forward Modeling: MSc Thesis, Central South University.

Zienkiewicz, O. C., 1977, The Finite Element Method, third edition: McGraw–Hill.

Appendix A: finite element formula

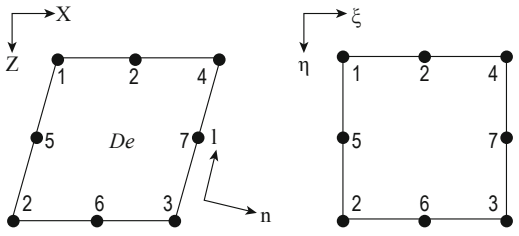

Fig. A-1 An eight-node isoparametric element. De is the domain of the element and ∂De represents the boundaries of the element, and l and n are tangential and normal vectors, respectively.

Figure A-1 shows an eight-node isoparametric element. In each element, the physical parameters σ, μ, and ε are constant. The global coordinates and each EM field component F are

$$x = \sum_{i=1}^{8} N_i^e x_i, \tag{A-1}$$

$$z = \sum_{i=1}^{8} N_i^e z_i, \tag{A-2}$$

$$\hat{F} = \sum_{i=1}^{8} N_i^e \hat{F}_i, \tag{A-3}$$

where, x_i, z_i, and $\hat{F}_i$ is the x-coordinate, z-coordinate, and EM field for one element and N_i^e is the shape function (Zienkiewicz, 1977)

$$N_1^e = \frac{1}{4}(1-\xi)(1+\eta)(-\xi+\eta-1), \tag{A-4}$$

$$N_2^e = \frac{1}{4}(1-\xi)(1-\eta)(-\xi-\eta-1), \tag{A-5}$$

$$N_3^e = \frac{1}{4}(1+\xi)(1-\eta)(\xi-\eta-1), \tag{A-6}$$

$$N_4^e = \frac{1}{4}(1+\xi)(1+\eta)(\xi+\eta-1), \tag{A-7}$$

$$N_5^e = \frac{1}{2}(1-\eta^2)(1-\xi), \tag{A-8}$$

$$N_6^e = \frac{1}{2}(1-\xi^2)(1-\eta), \tag{A-9}$$

$$N_7^e = \frac{1}{2}(1-\eta^2)(1+\xi), \tag{A-10}$$

$$N_8^e = \frac{1}{2}(1-\xi^2)(1+\eta). \tag{A-11}$$

We apply the Galerkin method to equations (6a) and (6b) and we obtain the equations

$$R^{\mathrm{H}} = \iint_{D_e} [N_i^e(-\frac{\partial}{\partial x}(p\frac{\partial \hat{H}_y^s}{\partial x}) - \frac{\partial}{\partial z}(p\frac{\partial \hat{H}_y^s}{\partial z}) - \frac{\partial}{\partial x}(-q\frac{\partial \hat{E}_y^s}{\partial z}) - \frac{\partial}{\partial z}(q\frac{\partial \hat{E}_y^s}{\partial x}) - i\omega\mu_0\hat{H}_y^s - \hat{S}_1)]dxdz = 0, \tag{A-12}$$

$$R^{\mathrm{E}} = \iint_{D_e} [N_i^e(-\frac{\partial}{\partial x}(q\frac{\partial \hat{H}_y^s}{\partial z}) - \frac{\partial}{\partial z}(-q\frac{\partial \hat{H}_y^s}{\partial x}) - \frac{\partial}{\partial x}(r\frac{\partial \hat{E}_y^s}{\partial x}) - \frac{\partial}{\partial z}(r\frac{\partial \hat{E}_y^s}{\partial z}) - \sigma\hat{E}_y^s - \hat{S}_2)]dxdz = 0. \tag{A-13}$$

From Green's theorem (Zienkiewicz, 1997)

$$\iint_{D_e} \phi\frac{\partial \varphi}{\partial x}dxdz = -\iint_{D_e} \frac{\partial \varphi}{\partial x}\phi dxdz + \oint_{\partial D_e} \phi\varphi n_x dl, \tag{A-14}$$

we obtain the following

$$\sum_{e=1}^{Ne}\iint_{D_e} [\frac{\partial N_i^e}{\partial x}(p\frac{\partial \hat{H}_y^s}{\partial x}) + \frac{\partial N_i^e}{\partial z}(p\frac{\partial \hat{H}_y^s}{\partial z}) + N_i^e(i\omega\mu_0\hat{H}_y^s) - \frac{\partial N_i^e}{\partial x}(q\frac{\partial \hat{E}_y^s}{\partial z}) + \frac{\partial N_i^e}{\partial z}(q\frac{\partial \hat{E}_y^s}{\partial x})]dxdz = \sum_{e=1}^{Ne} N_i^e\hat{S}_1 dxdz, \tag{A-15}$$

$$\sum_{e=1}^{Ne}\iint_{D_e} [\frac{\partial N_i^e}{\partial x}(q\frac{\partial \hat{H}_y^s}{\partial z}) - \frac{\partial N_i^e}{\partial z}(q\frac{\partial \hat{H}_y^s}{\partial x}) + N_i^e(\sigma\hat{E}_y^s) + \frac{\partial N_i^e}{\partial x}(r\frac{\partial \hat{E}_y^s}{\partial x}) + \frac{\partial N_i^e}{\partial x}(q\frac{\partial \hat{E}_y^s}{\partial x})]dxdz = \sum_{e=1}^{Ne} N_i^e\hat{S}_2 dxdz. \tag{A-16}$$

In any element, we have

$$\begin{bmatrix} \mathrm{K_H^e} & \mathrm{K_C^e} \\ \mathrm{K_C^{e\,T}} & \mathrm{K_E^e} \end{bmatrix}\begin{bmatrix} \mathrm{H} \\ \mathrm{E} \end{bmatrix} = \begin{bmatrix} \mathrm{U} \\ \mathrm{V} \end{bmatrix}, \tag{A-17}$$

$$K_C^{ij} = \iint_{D_e} (-q\frac{\partial N_i^e}{\partial x}\frac{\partial N_j^e}{\partial z} + q\frac{\partial N_i^e}{\partial z}\frac{\partial N_j^e}{\partial x})dxdz, \tag{A-18}$$

$$K_H^{ij} = \iint_{D_e} (p\frac{\partial N_i^e}{\partial x}\frac{\partial N_j^e}{\partial x} + p\frac{\partial N_i^e}{\partial z}\frac{\partial N_j^e}{\partial z} + i\omega\mu_0 N_i^e N_j^e)dxdz, \tag{A-19}$$

$$K_E^{ij} = \iint_{D_e} (r\frac{\partial N_i^e}{\partial x}\frac{\partial N_j^e}{\partial x} + r\frac{\partial N_i^e}{\partial z}\frac{\partial N_j^e}{\partial z} + \sigma N_i^e N_j^e)dxdz, \tag{A-20}$$

$$U_i = \iint_{D_e} N_i^e\hat{S}_1 dxdz, \tag{A-21}$$

$$V_i = \iint_{D_e} N_i^e\hat{S}_2 dxdz. \tag{A-22}$$

By assigning A-16 to the global matrix, we obtain the solution of the system of linear equations $\mathbf{K}\hat{\mathbf{F}} = \mathbf{B}$.

Appendix B: Jacobian matrix calculation

We used the VCX configuration to calculate the Jacobian matrix

$$\hat{\mathbf{J}}_{ij} = \frac{\partial \hat{H}_{xi}^s}{\partial \sigma_j}, \tag{B-1}$$

Because the air conductivity σ is zero, equation (9) can be written as

$$\hat{H}_x^s = q\frac{\partial \hat{H}_y^s}{\partial x}, \tag{B-2}$$

The derivatives of the magnetic field with respect to σ_j are

$$\frac{\partial \hat{H}_x^s}{\partial \sigma_j} = \frac{\partial q}{\partial \sigma_j}\frac{\partial \hat{H}_y^s}{\partial x} + q\frac{\partial}{\partial \sigma_j}\left(\frac{\partial \hat{H}_y^s}{\partial x}\right), \tag{B-3}$$

$$\frac{\partial \hat{H}_y^s}{\partial x} = \sum_{k=1}^{8}\frac{\partial N_k^e}{\partial x}\hat{H}_{yk}^s, \tag{B-4}$$

$$\frac{\partial}{\partial \sigma_j}\left(\frac{\partial \hat{H}_y^s}{\partial x}\right) = \sum_{k=1}^{8}\frac{\partial N_k^e}{\partial x}\frac{\hat{H}_{yk}^s}{\partial \sigma_j}. \tag{B-5}$$

According to the reciprocity principle

$$\frac{\partial}{\partial \sigma_j}\left(\frac{\partial \hat{H}_y^s}{\partial x}\right) = \sum_{k=1}^{16} W_k F_k^8, \tag{B-6}$$

$$\mathbf{W} = -\begin{bmatrix} \mathbf{K}_{\mathbf{H}}^{'} & \mathbf{K}_{\mathbf{C}}^{'} \\ \mathbf{K}_{\mathbf{C}}^{\mathbf{T}'} & \mathbf{K}_{\mathbf{E}}^{'} \end{bmatrix}\begin{bmatrix} \mathbf{H} \\ \mathbf{E} \end{bmatrix}, \tag{B-7}$$

where $\mathbf{K}_{\mathbf{H}}^{'} = \frac{\partial \mathbf{K}_{\mathbf{H}}^e}{\partial \sigma_j}$, $\mathbf{K}_{\mathbf{C}}^{'} = \frac{\partial \mathbf{K}_{\mathbf{C}}^e}{\partial \sigma_j}$, $\mathbf{K}_{\mathbf{C}}^{\mathbf{T}'} = \frac{\partial \mathbf{K}_{\mathbf{C}}^{e\,\mathrm{T}}}{\partial \sigma_j}$, $\mathbf{K}_{\mathbf{E}}^{'} = \frac{\partial \mathbf{K}_E^e}{\partial \sigma_j}$, and $\mathbf{H} = \begin{bmatrix} \hat{H}_{y1}^s & \cdots & \hat{H}_{y8}^s \end{bmatrix}^{\mathrm{T}}$ and $\mathbf{K}_{\mathbf{H}}^e$, $\mathbf{K}_{\mathbf{C}}^e$, $\mathbf{K}_{\mathbf{C}}^e$, and $\mathbf{K}_{\mathbf{E}}^e$ are elemental matrices (for details see Appendix A). **H** and **E** correspond to the magnetic and electric field for the eight-node element with respect to the conductivity of a particular block σ_j. F_k^8 represents the magnetic and electric fields in the eight-node element with respect to the conductivity of a particular block σ_j owing to the unit source at the receiver point.

Li Wen-Ben: Ph.D. candidate, he graduated from Jilin University in 2011. His main research interests are electromagnetic forward modeling and inversion.